DIFFRACTION ANALYSIS FOR THE SORTYM FORMATION USING VERTICAL SEISMIC PROFILING DATA

ALEXANDER KLOKOV[1], DAMIR IRKABAEV[2], OSARENI OGIESOBA[1], KONSTANTIN SKACHEK[3] and NAIL MUNASYPOV[4]

[1] *Bureau of Economic Geology, The University of Texas at Austin, University Station, Box X, Austin, TX 78713-8924, U.S.A. alexander.klokov@gmail.com*
[2] *SPC Geostra, 3 Luganskaya St., Ufa, Republic of Bashkortostan, 450071 Russia.*
[3] *LUKOIL - West Siberia, 20 Pribaltiyskaya St., Kogalym, Khanty-Mansi Autonomous District - Yugra, Tyumen region, 628486 Russia.*
[4] *Bashneftegeofizika, 13 Lenina St., Ufa, Republic of Bashkortostan, 450000 Russia.*

(Received July 18, 2014; revised version accepted September 21, 2014)

ABSTRACT

Klokov, A., Irkabaev, D., Ogiesoba, O., Skachek, K. and Munasypov, N., 2014. Diffraction analysis for the Sortym Formation using vertical seismic profiling data. *Journal of Seismic Exploration*, 23: 463-480.

Seismic diffraction analysis may be a strong supplement for interpretation workflows. It allows characterization of small geologic features, which may not be detectable by conventional attribute analysis. Diffractions can play a significant role in fracture detection and characterization.

In this work, we extract seismic diffractions from vertical seismic profiling (VSP) data acquired within the Sortym Formation in West Siberia. Seismic images of scattering objects were constructed for three components of the wavefield. We interpret the multicomponent diffraction images, comparing them with instantaneous frequency and instantaneous amplitude derived from conventional migrated data. The diffraction analysis allowed us to refine composition of the strata, to detect fracture clusters, and to predict the cluster orientation.

KEY WORDS: diffraction imaging, borehole geophysics, VSP, multicomponent, shear waves, interpretation, fracture, shale.

INTRODUCTION

Seismic interpretation is traditionally based on reflection energy analysis. A seismic image depicts reflection boundaries. Faults are interpreted by reflectors breaking. Widely used seismic attributes, which are transformations of reflection coefficients, usually are obtained along reflection horizons.

0963-0651/14/$5.00

Along with reflections, a seismic wavefield contains the diffracted component - waves emitted from reflector edges or scattered by small-scale geologic inhomogeneities. The inhomogeneity may be a small geologic object like a pinch-out or fracture; or it may be a local change in petrophysical properties. Diffractions assist seismic interpretation by revealing features that are not imaged by conventional migration approaches due to their small size or that are not detectable by seismic attributes due to their small distinction in reflection properties. Using separated diffracted waves may play a primary role in fracture detection and characterization, which are crucial for exploration and production.

Despite their high potential, diffractions are not widely used in interpretation workflows, probably because of their low energy. Diffraction analysis is challenged by the tremendous difference in energy between diffracted waves and reflected waves (Klem-Musatov, 1994). Frequently, diffractions are completely suppressed by strong reflections. Moreover, the signal from weak scatterers may be distorted by different noises.

Recently, however, interest in diffractions has been on a steady rise. Several different techniques for diffraction extraction have been developed and applied to seismic data interpretation (Kozlov et al., 2004; Berkovitch et al., 2009; Al-Dajani and Fomel, 2010; Burnett and Fomel, 2011; Koren and Ravve, 2011; Tsingas et al., 2011; Klokov and Fomel, 2012; Asgedom et al., 2013; Alonaizi et al., 2013; Gelius et al., 2013; Sturzu et al., 2014; Zhang and Zhang, 2014).

In addition to analyzing diffractions from the surface seismic wavefield, vertical seismic profiling (VSP) has great potential for seismic diffraction analysis. This technology involves placing seismic receivers deep into wells, allowing the receivers to be located much closer to scattering bodies, which preserves both the power and the high-frequency content of the signal (Hardage, 2000).

The diffraction component of VSP data has attracted attention in recent years. Moser et al. (2000) constructed diffractivity depth sections, running migration with opposite weights, and separated diffractions by a cascade of f-k and median filters. Nikitchenko et al. (2008) imaged scattering objects using cross-correlation stacking and NMO enhancement. Nikitchenko et al. (2011) discussed diffraction imaging for cross-well seismic data. Three-component borehole sensors provide the opportunity for registration and analysis of both compressional and shear waves. Meadows and Winterstein (1994) analyzed shear-wave diffractions to monitor hydraulic fractures. Liu et al. (1997) presented the theory of diffraction of seismic waves by fractures. Bellefleur et al. (2004) described scattering from massive sulfide ore bodies. Humphries (2009) located diffractors using particle motion analysis and used diffraction energy to orient VSP receivers (Humphries, 2010).

In this study, we perform diffraction analysis for VSP data acquired within the Sortym Formation in West Siberia. Multicomponent data provide the opportunity to construct and analyze a separate diffraction image for each component. Joint analysis of the components allows validation of imaged scatterers. To interpret the diffraction images, we adopted an integrated approach by considering results from instantaneous frequency and instantaneous amplitude derived from conventional migrated data. We have also taken into account the geological background of the formation.

GEOLOGICAL BACKGROUND

The geologic formation of interest is composed of clastic sediments, which are typical of West Siberia, as revealed by a vertical borehole. The productive part of the formation consists of a thick sandstone and shale sequence divisible into two units, upper and lower. The upper unit is composed mostly of interbedded sandstones and siltstones. The lower unit, which is the oil-saturated interval, is composed dominantly of mudstone, within which are interbedded sandstone and argillaceous sandstone layers that pinch out laterally. The lower unit is characterized by strong lateral lithological variations. Some of the sandstone beds appear to be wedges tapering into mudstone; some are of uniform thickness and relatively continuous but grade gradually into mudstone, while others terminate abruptly and are less continuous. Three oil-saturated intervals consisting of two sandstone beds and one argillaceous sandstone bed were identified within this unit in our study area. The argillaceous sandstone interval is overlain by a bituminous shale bed - the Bazhenov Formation.

Although the oil-saturated lower unit in our study area exhibits strong lateral lithologic variations, it is characterized seismically by weak contrast in elastic properties associated with the sandstone and siltstone beds, compared with larger contrasts associated with the encasing mudstone. In addition, the encasing mudstone, which acts as the sealing rock, has strong influence on vertical velocity.

DATA ACQUISITION

The VSP data were collected from explosive sources located at three different azimuths, with offsets of about 1300 m. One zero-offset source was used for velocity estimation. The acquisition geometry is outlined in Fig. 1.

The data registration was performed by a 148-level three-component tool with 20 m spacing between the receivers. Receiver stations were placed between 40 and 2980 m in depth. The record length was 4 s with a 1 ms sample rate.

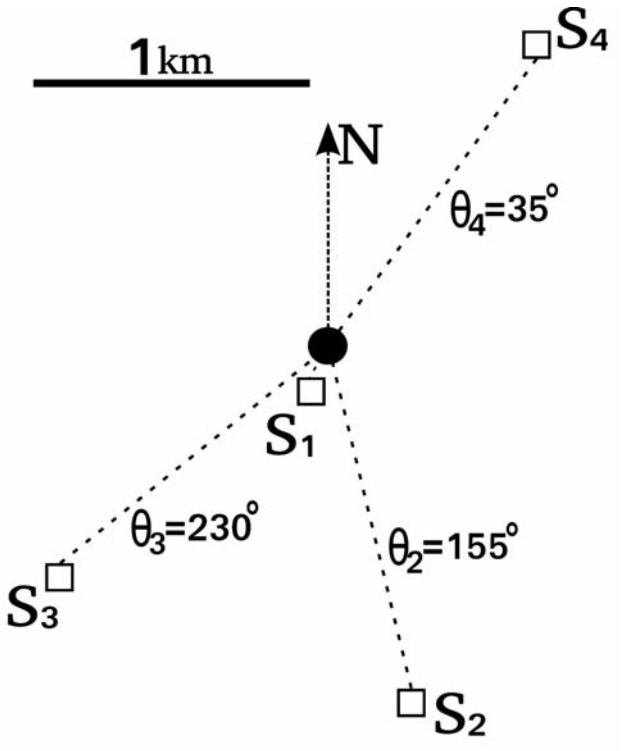

Fig. 1. Acquisition geometry. The borehole is the black dot. Source locations are shown by the squares.

RESULTS

Figs. 2-4 compare depth sections for the three VSP data components and for all three source azimuths. Because sources S3 and S4 are almost along the same line, we present images from both source directions on the same panel, while the image from the S2 direction is shown on a separate panel. The compressional component (Fig. 2) clearly shows horizontal bedding. Strong reflection from the Bazhenov Formation dominates at a depth of about 2.82 km. Shear waves, in turn, appear to reveal a large amount of discontinuities and inhomogeneities along reflection boundaries (Figs. 3 and 4).

Figs. 5-7 compare instantaneous frequency sections obtained from the conventional reflection images. We indicated negative values by a contrasting color, following Hardage et al. (1998), who discussed anomalous values of instantaneous frequency as valuable indicators of stratigraphic terminations. This attribute confirms the complexity of the formation because all sections are densely filled by negative frequencies. Figs. 8-10 show instantaneous amplitude sections.

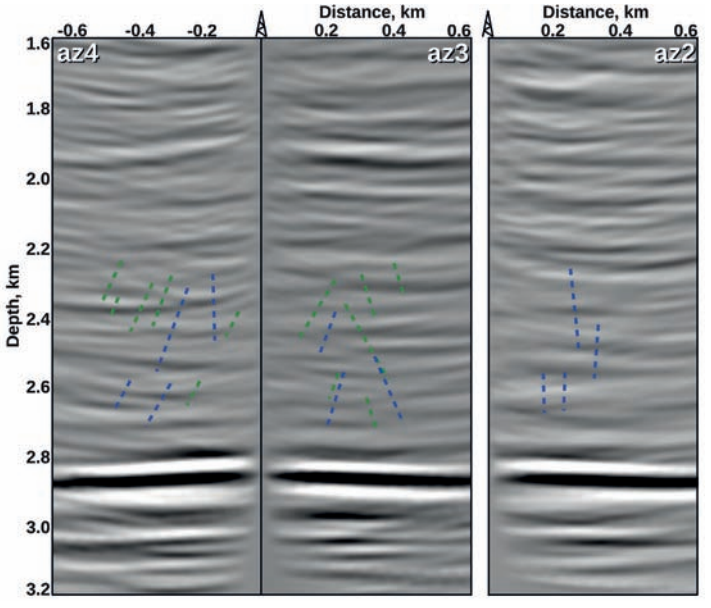

Fig. 2. Depth images for the compressional component. The dash lines indicate fracture clusters interpreted on diffraction images for the radial (green) and the transverse (blue) components. "azN" means the azimuth to source station N.

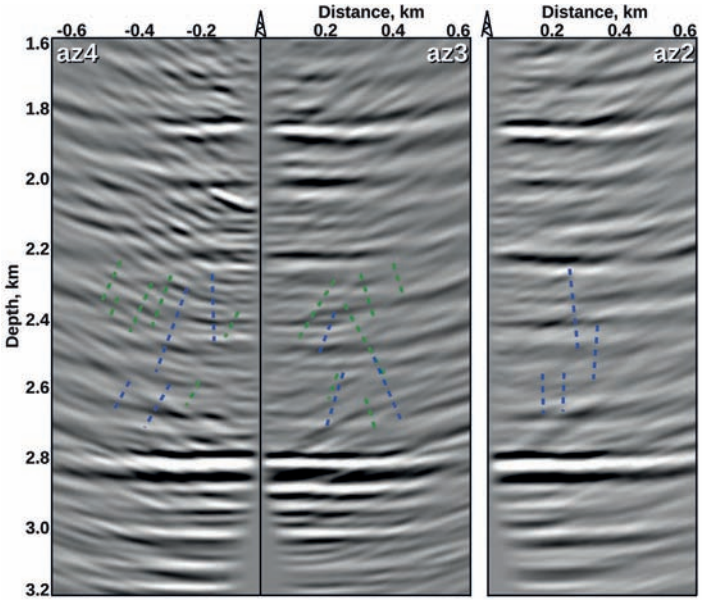

Fig. 3. Depth images for the radial component. The dash lines indicate fracture clusters interpreted on diffraction images for the radial (green) and the transverse (blue) components. "azN" means the azimuth to source station N.

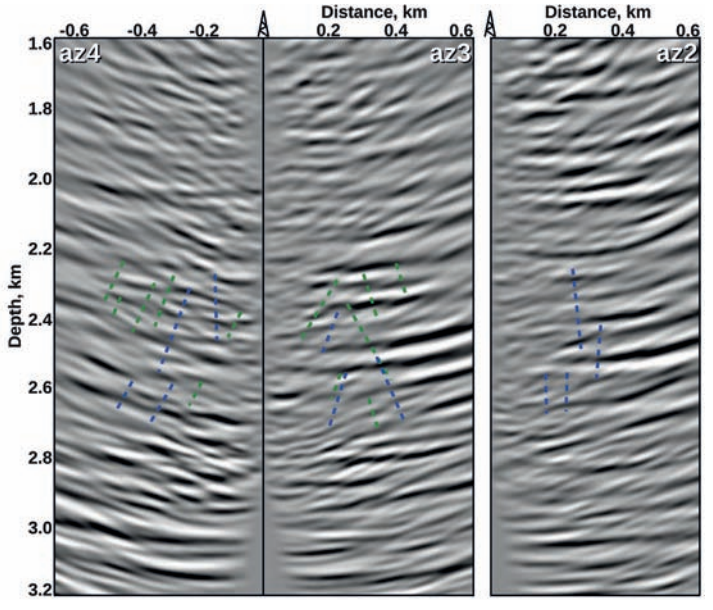

Fig. 4. Depth images for the transverse component. The dash lines indicate fracture clusters interpreted on diffraction images for the radial (green) and the transverse (blue) components. "azN" means the azimuth to source station N.

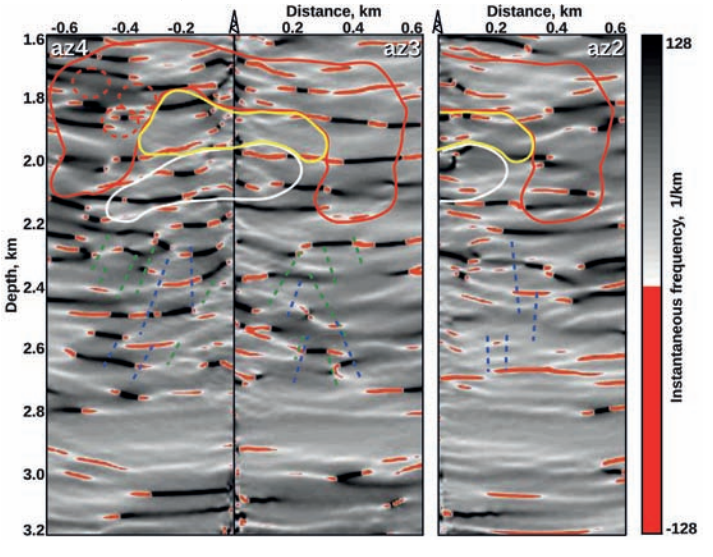

Fig. 5. Instantaneous frequency for the compressional component. The dash lines indicate fracture clusters interpreted on diffraction images for the radial (green) and the transverse (blue) components. The solid lines show zones with different diffraction properties. "azN" means the azimuth to source station N.

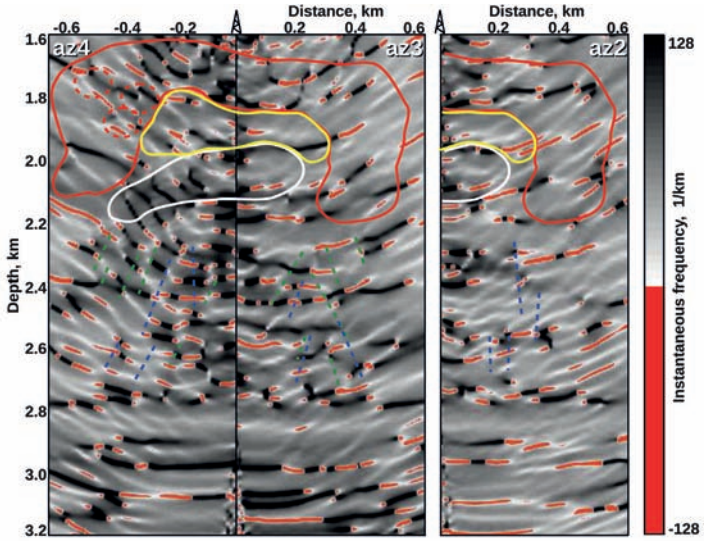

Fig. 6. Instantaneous frequency for the radial component. The dash lines indicate fracture clusters interpreted on diffraction images for the radial (green) and the transverse (blue) components. The solid lines show zones with different diffraction properties. "azN" means the azimuth to source station N.

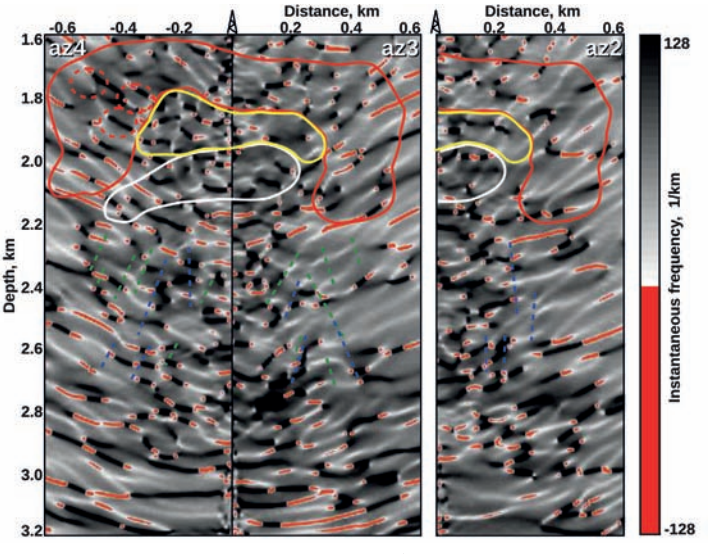

Fig. 7. Instantaneous frequency for the transverse component. The dash lines indicate fracture clusters interpreted on diffraction images for the radial (green) and the transverse (blue) components. The solid lines show zones with different diffraction properties. "azN" means the azimuth to source station N.

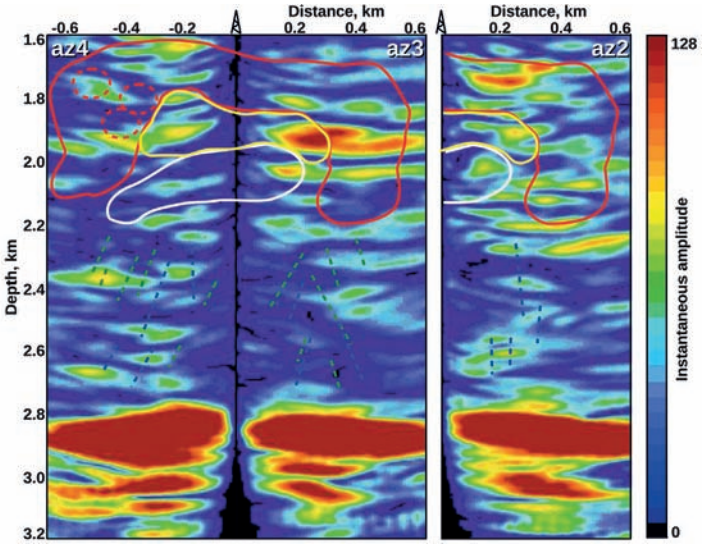

Fig. 8. Instantaneous amplitudes for the compressional component. The dash lines indicate fracture clusters interpreted on diffraction images for the radial (green) and the transverse (blue) components. The solid lines define zones with different diffraction properties. "azN" means the azimuth to source station N.

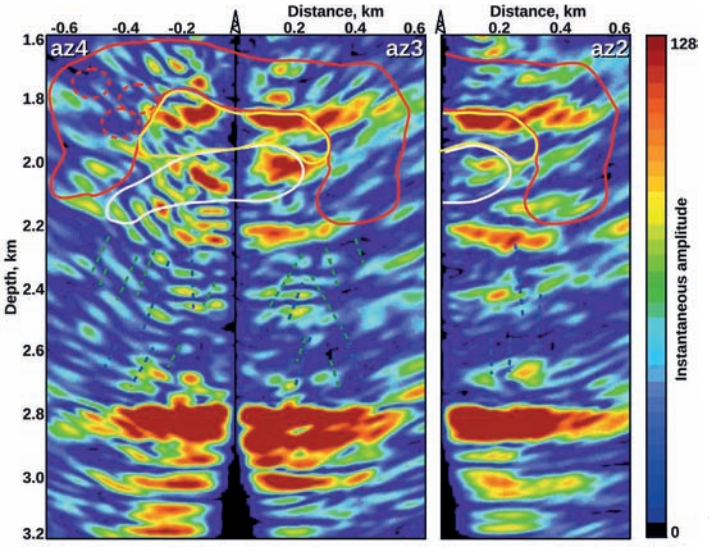

Fig. 9. Instantaneous amplitudes for the radial component. The dash lines indicate fracture clusters interpreted on diffraction images for the radial (green) and the transverse (blue) components. The solid lines define zones with different diffraction properties. "azN" means the azimuth to source station N.

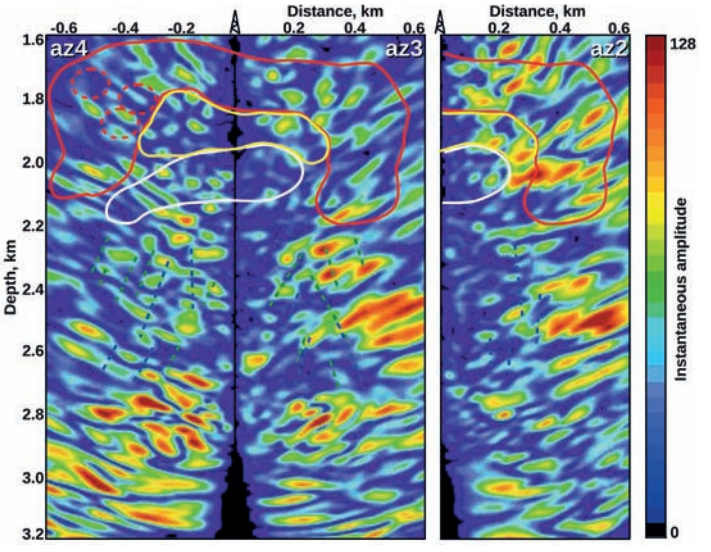

Fig. 10. Instantaneous amplitudes for the transverse component. The dash lines indicate fracture clusters interpreted on diffraction images for the radial (green) and the transverse (blue) components. The solid lines define zones with different diffraction properties. "azN" means the azimuth to source station N.

To minimize possible distortion of the diffraction component, we limited preliminary data processing by rotation of the recorded VSP data and separation of the upgoing wavefield.

To extract diffractions we adapted the method described by Klokov and Fomel (2012). The horizontal bedding allowed us to easily eliminate reflections - we picked the strongest reflection from the Bazhenov Formation and destroyed all events parallel to that. Then, the residual data were migrated into the dip-angle domain (Koren and Ravve, 2011). Migration velocities were obtained from the first-break times. Finally, we used the Radon transform to separate diffraction events from noise. Stacking of the filtered migrated gathers over the dip angle provided diffraction images. The procedure was performed separately for each data component.

The diffraction images are shown in Figs. 11-13. Although only a single source has been used, the diffraction sections reveal large amounts of scattering objects, which demonstrates the high potential of borehole seismic methods for diffraction analysis. However, the single source also has generated strong imaging artifacts. Specifically, the scatterers are imaged as extended strokes,

which have different slopes for compressional and shear waves. The difference in slopes is due to the velocity differences among the components.

The artifacts complicate interpretation of the diffraction images and correlation among the components. However, one may observe agreement among the sections. Red circles at a depth of about 1.8 km indicate a set of objects that is clearly imaged by all three components.

The diffraction imaging approach used means the processing of migrated gathers. Analysis of events in the processed gathers is an alternative way to validate the diffraction images. Exactly at the position of the scattering object, diffraction events are flat (Klokov and Fomel, 2012). However, at locations away from the scatterer, diffraction events exhibit some amount of slope. Diffraction images are supposed to have this "flat-slope" signature in dip-angle gathers.

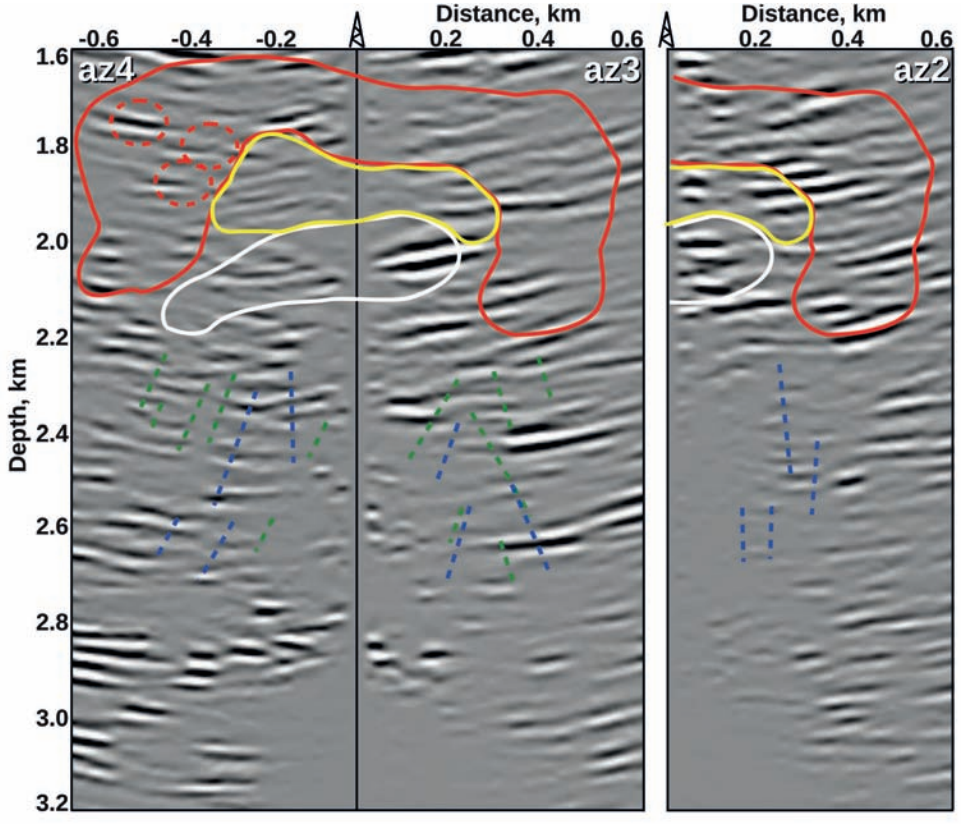

Fig. 11. Diffraction images for the compressional component. The dash lines indicate fracture clusters interpreted on the radial (green) and the transverse (blue) components. The solid lines define zones with different diffraction properties. "azN" means the azimuth to source station N.

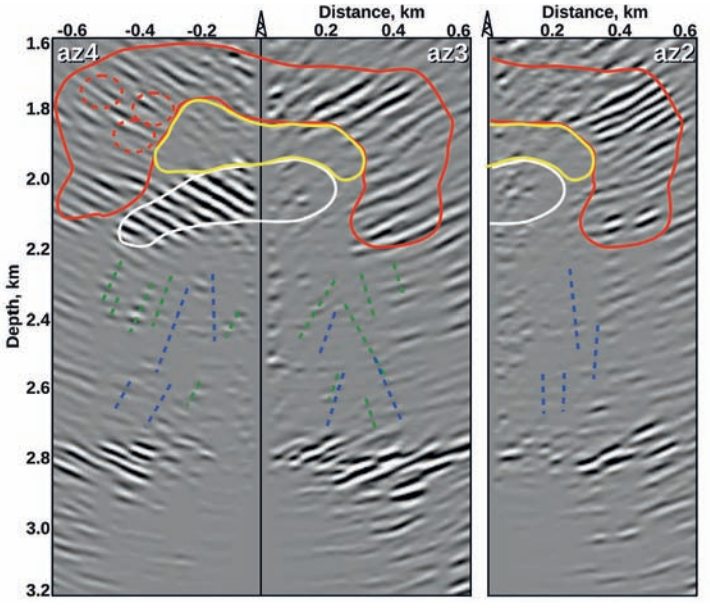

Fig. 12. Diffraction images for the radial component. The dash lines indicate fracture clusters interpreted on the radial (green) and the transverse (blue) components. The solid lines define zones with different diffraction properties. "azN" means the azimuth to source station N.

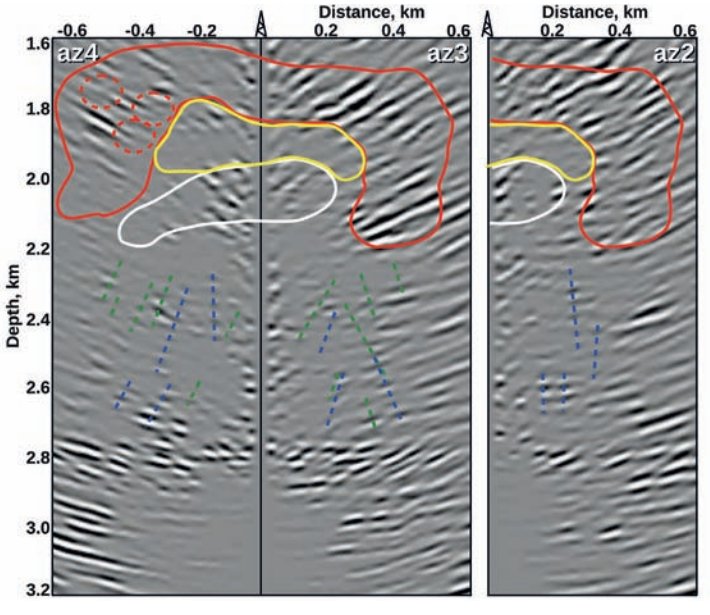

Fig. 13. Diffraction images for the transverse component. The dash lines indicate fracture clusters interpreted on the radial (green) and the transverse (blue) components. The solid lines define zones with different diffraction properties. "azN" means the azimuth to source station N.

Fig. 14 shows a part of the diffraction image for the radial component and two processed dip-angle gathers. The red crossing lines in the image depict a point object, which is a part of the near-vertical sequence. At the migrated gather observed just above the object (Fig. 14b), one may detect a flat event at a depth level of the object. At the gather taken from 20 m away, the same event appears inclined. This observation supports interpretation of the considered imaged point as a scattering small-scale geologic feature.

For comparison, Fig. 15 shows a conventional depth-migrated image and two migrated gathers from the same positions. The near-vertical sequence and the diffraction event in the migrated gathers are not clearly visible because of dominating reflected energy.

DIFFRACTION ANALYSIS

Scattering objects are not distributed evenly in the diffraction images (Figs. 11-13 and 16-17). One may observe, especially in shear-wave sections, depth intervals with stronger diffractivity, while some intervals are relatively quiet. One also may note that the distribution of diffractions is consistent with interval velocities. Below, we interpret the diffraction images within the constant-interval-velocity layers.

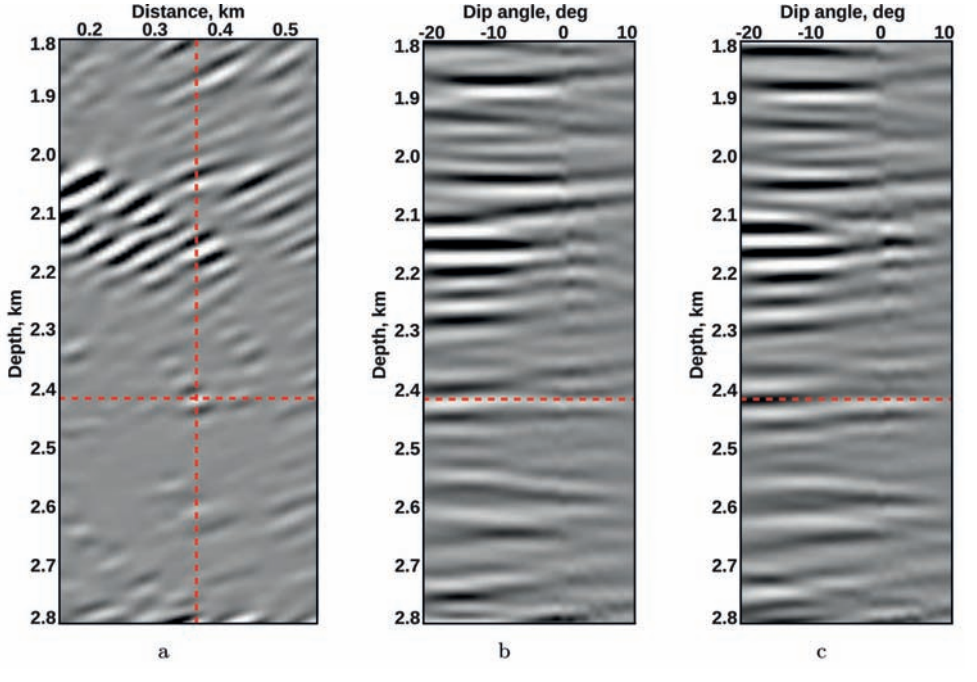

Fig. 14. (a) Diffraction image and processed dip-angle gathers for (b) position above the scattering object and (c) position 20 m away.

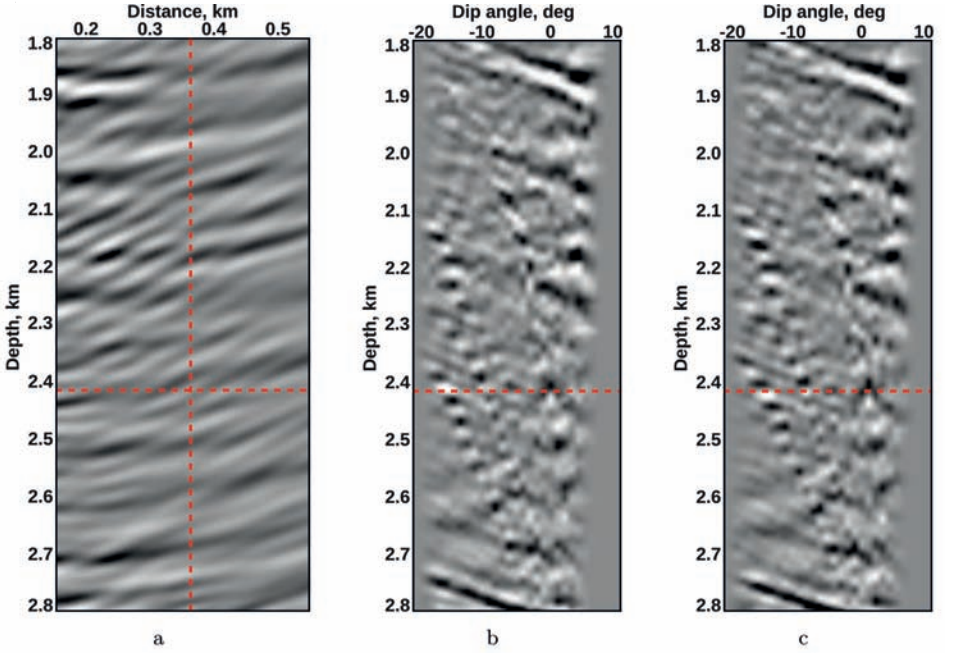

Fig. 15. Depth-migrated image and dip-angle gathers for (b) position above the scattering object and (c) position 20 m away.

Lenticular bedding

Diffraction imaging reveals many strong diffractors at the depth interval of 1.6 - 2.2 km. The diffractors may be gathered to several clusters.

At about 1.7 km depth, the diffraction sections show an extended area of strong diffractivity (shown in red). The shear waves more distinctly depict outlines of the area. Note that the outlines coincide at azimuths 2 and 3: thickness of the diffraction accumulation increases as the distance from the borehole increases. Both the radial and the transverse components reveal local increase of scattering power at the offset of 0.4 km. In this depth interval, the conventional images show strong reflection boundaries (Fig. 3) with rapidly changing amplitudes (Fig. 9). The area contains positive frequencies, frequency terminations, and negative frequencies (Figs. 6-8). Diffractions do not show strong correlation with negative frequencies, although some areas characterized by frequency terminations (that is, areas where positive frequencies change to negative frequencies) are coincident with diffractions.

Another accumulation of diffractors may be seen at about 2.1 km depth (shown in white). The radial component exposes very strong diffractors at azimuth 4 (Fig. 16). The area is characterized by high amplitudes of the radial

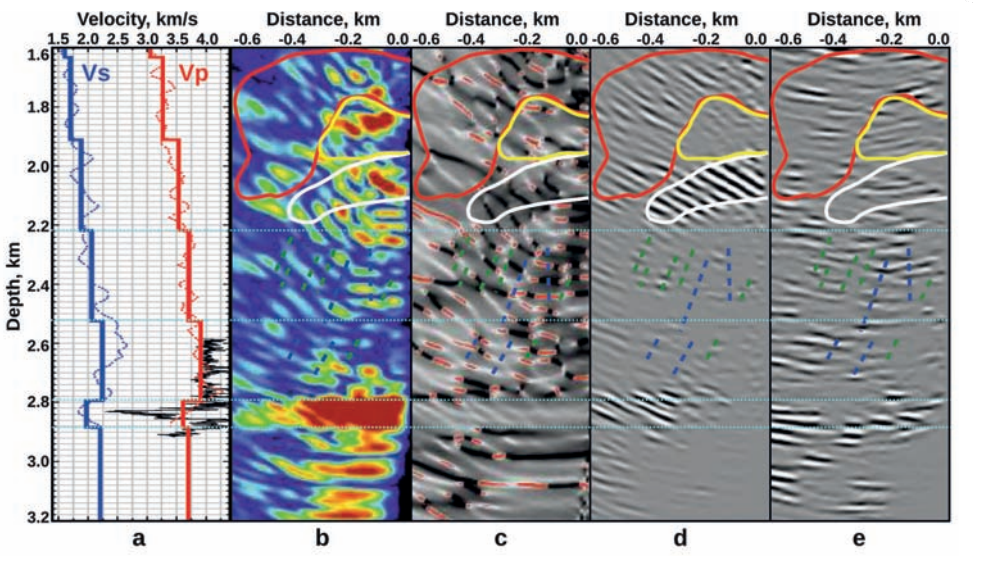

Fig. 16. Attribute sections for azimuth 4 tied to the velocity profile. (a) Interval velocities (solid lines) for compressional and shear waves and instantaneous velocities (dotted lines). Acoustic log is plotted in black. (b) Instantaneous amplitude for the radial component. (c) Instantaneous frequency for the radial component. (d) Diffraction image for the radial component. (e) Diffraction image for the compressional component.

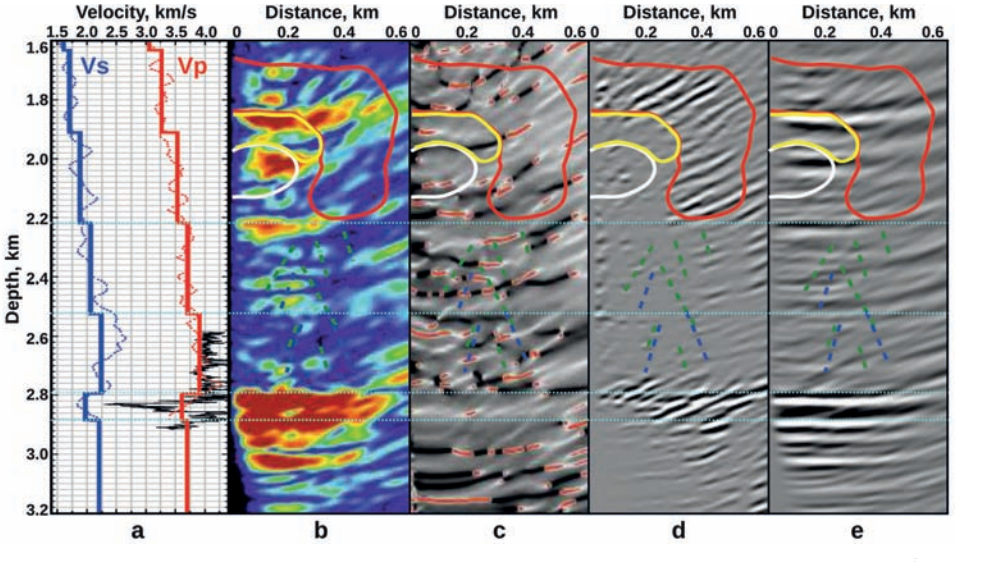

Fig. 17. Attribute sections for azimuth 3 tied to the velocity profile. (a) Interval velocities (solid lines) for compressional and shear waves and instantaneous velocities (dotted lines). Acoustic log is plotted in black. (b) Instantaneous amplitude for the radial component. (c) Instantaneous frequency for the radial component. (d) Diffraction image for the radial component. (e) Conventional image for the radial component.

component. Frequency content is mostly positive, changing from high values at the left side to moderate values at the right. The compressional and the transverse components look less sensitive to the diffracting body - amplitudes are moderate and many negative frequencies are detected. The area that separates these two diffraction clusters (shown in yellow) looks more quiet in the diffraction images. It contains strong amplitudes, and its frequency content is mostly positive.

We attribute the main part of the imaged scatterers at the upper cluster (red outline) to strong stratigraphical variation within the formation. Lenticular bedding and pinch-outs are heterogeneities whose impedance contrast causes strong scattered seismic waves. The yellow outline indicates more consolidated interlayers. The high diffractivity at the bottom cluster (white outline) may be caused by a combination of stratigraphical variations and fracturing. The overlying compacted rock may contribute fluid saturation that greatly increases scattering power.

Fracture clusters

Diffractors at the interval of 2.2 - 2.5 km may be interpreted differently. These kinds of scatterers are clearly shown by the shear waves: objects interpreted at the radial diffraction image are shown in green, and objects indicated by the transverse component are shown in blue. These diffractors are all subvertical and are characterized by low amplitudes (Figs. 8-10). Many appear to be associated with areas where reflections exhibit no displacement. The interpreted scatterers may also be seen in the compressional diffraction images; however, these sections are much less resolved.

Due to the geometry and low reflected amplitudes, we attribute these diffraction objects to fracture clusters that occur at certain locations within the interval. The diffractors dominate along the directions of sources 3 and 4; only a few are in the source 2 direction. This observation suggests the direction of fracturing: the clusters are extended along the source 2 direction. Note that the clusters are not clearly shown by frequencies.

Compacted rock

Lensky and Akhtyamov (2012) preliminarily analyzed the core taken within the 2.5 - 2.8 km interval; no fractures were identified. As confirmation, the interval has the highest rate of velocity. One may observe vertical diffraction objects, but there are fewer than in the overlying layers. We interpret the interval as the most compacted mudstone. The high resistance of the strata provides oil saturation of two contained sandstone layers and the underlying shale.

Oil-saturated shale

The interval of 2.8 - 2.9 km demonstrates a large number of strong scatterers, which are distributed almost evenly from near to far offsets. Reflections show no displacement; frequencies are mostly very low and positive. The strong diffractivity is confined to the thickness of the interval; there are almost no strong diffractors below 2.9 km.

Lensky and Akhtyamov (2012) reported anisotropy at this depth interval. From shear-wave splitting analysis, they showed that the dominant fracture orientation was 325 degrees. The interpretation was validated by core analysis: samples from the anisotropic interval displayed a large number of vertical fractures. We correlate the diffractivity with fracturing within the layer reported by the previous study. The high diffraction energy is caused by oil saturation of the fractures, which provides high impedance contrast.

Note that these strong diffractions differ from strong diffractions observed in the top interval. Diffractions associated with lenticular bedding are accompanied by negative frequencies. The oil-saturated interval, where diffractions originate from fractures, has positive frequency content. Diffraction analysis potentially could provide evidence of fracture orientation. Patterns of diffractors observed at all diffraction sections may be used to detect or validate fracturing direction. However, the limited frequency content of the considered data and the single source do not allow more detailed characterization.

DISCUSSION AND CONCLUSION

Vertical seismic profiling data contain a large number of scattered waves that may be extracted and studied. Diffraction analysis can be a strong support for conventional interpretation techniques and can provide additional information to characterize small-scale features. The result of attribute analysis, as image processing, may be distorted by strong imaging noise. This is especially true for VSP acquisition geometry. Diffraction analysis, however, uses unmigrated data as input and provides alternative interpretable information. Agreement between attributes and diffractions may be valuable in complicated cases. At the same time, disagreement between the two approaches may motivate the interpreter to conduct further investigation and thus prevent potential errors. In addition, diffractions may accentuate some features not clearly visible after conventional data processing.

Diffraction analysis provides the opportunity to refine weak seismic waves, which makes diffractions useful for faulting and fracturing interpretation. Diffractions allow imaging of fracture clusters or even single fractures. They may allow detection of fracture orientation when working with azimuthal 2D

lines: fracture patterns that are traceable in several sections are a great indicator of fracture orientation.

Offset VSP-data diffraction imaging is susceptible to distortions caused by the limitations of 2D VSP acquisition geometry. Borehole sensors may register diffractions originating from out-of-plane scattering points. Conventional migration does not filter out these objects but instead projects them to the imaging section at incorrect positions. The positioning error increases as the distance of the object from the plane increases (Biondi, 2006; Hobbs et al., 2006). The three data components recorded in VSP acquisition allow polarization analysis and directional filtering to be done (Benhama et al., 1988; Morozov and Smithson, 1996; Diallo et al., 2005). However, the weakness of a diffracted signal may be the challenge for accurate direction detection. In this work, we did not take into consideration the possible deviation of the scattering objects. We supposed that scattered waves from highly remote objects were attenuated due to the preliminary data rotation and longer travel path.

In this work, we used a single source for each azimuth and revealed many scatterers. Walkaway VSP should enhance diffraction analysis power. Stacking of sources allows accumulation of weaker signals, which in turn means detection of more subtle objects. In addition, walkaway VSP data should reduce the imaging artifacts. Due to the limited acquisition, diffractors were imaged as extended strokes. In addition to velocity, the stroke length and slope are defined by the source position. Stacking of diffraction images from many sources allows accumulation of the signal at the correct diffractor position and reduction of the strokes. The effect of out-of-plane scatterers should be attenuated, as well.

A strong advantage of VSP acquisition is registration of shear waves, which appear to be more sensitive to small geological features. In our study, the radial component was the most meaningful. It allowed us to both delineate the area with strong stratigraphical variations and detect fracture clusters. Compressional and shear waves characterize scattering objects in different ways. Some objects may be visible in just one component while invisible in the others. Multicomponent diffraction imaging may significantly extend understanding of the subsurface features.

ACKNOWLEDGMENTS

We thank Valentina Bogdanova, Bob Hardage, and Vladimir Lensky for many fruitful discussions.

REFERENCES

Al-Dajani, A. and Fomel, S., 2010. Fractures detection using multi-azimuth diffractions focusing measure: Is it feasible? Expanded Abstr., 80th Ann. Internat. SEG Mtg., Denver, 29: 287.

Alonaizi, F., Pevzner, R., Bona, A. and Gurevich, B., 2013. 3D diffraction imaging of linear features and its application to seismic monitoring. Geophys. Prosp., 61: 1206-1217.

Asgedom, E., Gelius, L.-J. and Tygel, M., 2013. 2D common-offset traveltime based diffraction enhancement and imaging. Geophys. Prosp., 61: 1178-1193.

Bellefleur, G., Muller, C., Snyder, D. and Matthews, L., 2004. Downhole seismic imaging of a massive sulfide orebody with mode-converted waves, Halfmile Lake, New Brunswick, Canada. Geophysics, 69: 318-329.

Benhama, A., Cliet, C. and Dubesset, M., 1988. Study and applications of spatial directional filtering in three-component recordings. Geophys. Prosp., 36: 591-613.

Berkovitch, A., Belfer, I., Hassin, Y. and Landa, E., 2009. Diffraction imaging by multifocusing. Geophysics, 74: WCA75-WCA81.

Biondi, B.L., 2006. 3D Seismic Imaging. SEG, Tulsa, OK, 224 pp.

Burnett, W. and Fomel, S., 2011. Diffraction imaging using 3D azimuthally-anisotropic velocity continuation. Extended Abstr., 73rd EAGE Conf., Vienna.

Diallo, M., Kulesh, M., Holschneider, M. and Scherbaum, F., 2005. Instantaneous polarization attributes in time-frequency domain and wavefield separation. Geophys. Prosp., 53, 723-731.

Gelius, L., Tygel, M., Takahata, A., Asgedom, E. and Serrano, J., 2013. High-resolution imaging of diffractions - A window-steered MUSIC approach. Geophysics, 78: S255-S264.

Hardage, B.A., 2000. Vertical Seismic Profiling. Part I - Principles. Pergamon Press, New York.

Hardage, B.A., Pendleton, V., Simmons, J., Stubbs, B. and Uszynski, B., 1998. 3-D instantaneous frequency used as a coherency/continuity parameter to interpret reservoir compartment boundaries across an area of complex turbidite deposition. Geophysics, 63: 1520-1531.

Hobbs, R.W., Drummond, B.J. and Goleby, B.R., 2006. The effects of three-dimensional structure on two-dimensional images of crustal seismic sections and on the interpretation of shear zone morphology. Geophys. J. Internat., 164: 490-500.

Humphries, M., 2009. Locating VSP diffracted arrivals using a microseismic approach. Expanded Abstr., 79th Ann. Internat. SEG Mtg., Houston: 4184-4188.

Humphries, M., 2010. Orient VSP receivers using diffracted energy. Extended Abstr., 72nd EAGE Conf., Barcelona.

Klem-Musatov, K., 1994. Theory of Seismic Diffractions. SEG, Tulsa, OK, 410 pp.

Klokov, A. and Fomel, S., 2012. Separation and imaging of seismic diffractions using migrated dip-angle gathers. Geophysics, 77: S131-S143.

Koren, Z. and Ravve, I., 2011. Full-azimuth subsurface angle domain wavefield decomposition and imaging. Part I: Directional and reflection image gathers. Geophysics, 76: S1-S13.

Kozlov, E., Barasky, N., Korolev, E., Antonenko, A. and Koshchuk, E., 2004. Imaging scattering objects masked by specular reflections. Expanded Abstr., 74th Ann. Internat. SEG Mtg., Denver, 23: 1131-1134.

Lensky, V. and Akhtyamov, R., 2012. Fracture detection and characterization using offset vertical seismic profiling data. Karotazhnik (in Russian), 213: 83-91.

Liu, E., Crampin, S. and Hudson, J., 1997. Diffraction of seismic waves by cracks with application to hydraulic fracturing. Geophysics, 62: 253-265.

Meadows, M. and Winterstein, D., 1994. Seismic detection of a hydraulic fracture from shearwave VSP data at Lost Hills Field, California. Geophysics, 59: 11-26.

Morozov, I. and Smithson, S., 1996. Instantaneous polarization attributes and directional filtering. Geophysics, 61: 872-881.

Moser, T.J., Petersen, S. and Landa, E., 2000. Diffractivity analysis of VSP data. Expanded Abstr., 70th Ann. Internat. SEG Mtg., Calgary, Alberta: 758-761.

Nikitchenko, A., Kiyashchenko, D., Kashtan, B. and Troyan, V., 2011. Diffraction imaging with cross-well seismic data. Extended Abstr., 73nd EAGE Conf., Vienna.

Nikitchenko, A., Kiyashchenko, D., Kiselev, Y. and Kashtan, B., 2008. Imaging of scattering objects with VSP data - cross-correlation stacking and NMO enhancement. Extended Abstr., 70th EAGE Conf., Rome.

Sturzu, I., Popovici, A.M. and Moser, T.J., 2014. Diffraction imaging using specularity gathers. J. Seismic Explor., 23, 1-18.

Tsingas, C., Marhfoul, B.E., Satti, S. and Dajani, A., 2011. Diffraction imaging as an interpretation tool. First Break, 29: 57-61.

Zhang, J. and Zhang, J., 2014. Diffraction imaging using shot and opening-angle gathers: A prestack time migration approach. Geophysics, 79: S23-S33.